WEIGHT SELECTION BY MISFIT SURFACES FOR LEAST SQUARES ESTIMATION

by

Garrett Saunders

A Thesis

submitted in partial fulfillment

of the requirements for the degree of

Master of Science in Mathematics

Boise State University

March 2009

The Thesis presented by *Garrett Saunders* entitled *Weight Selection by Misfit Surfaces for Least Squares Estimation* is hereby approved.

Jodi Mead, Advisor	Date
Mary Jarratt Smith, Committee Member	Date
Grady Wright, Committee Member	Date
Steven Brill, Committee Member	Date
John R. Pelton, Graduate Dean	Date

ABSTRACT

Current hydrological methods used to predict ground water recharge rates rely on numerical solutions of the Richards equation which models the near surface unsaturated flow of water in porous soils. To effectively compute these solutions accurate information of a soil's ability to conduct water, known as hydraulic conductivity, is required. We anticipate that robust and cost efficient methods for measuring hydraulic conductivity are forthcoming, and hence propose a new method of data fitting using a quadratic cost function containing a weighted parameter and data misfit. Mead [5] employs an algorithm to compute the weight on the parameter misfit when the data, data weight, and a priori initial parameter estimate are specified. However, robust numerical codes are in place only for a simplified diagonal matrix on the parameter weight [6]. This diagonal weight is typically chosen to be an approximation to the l^{th} order derivative, and weights each parameter equally. This is insufficient for parameters of differing magnitudes such as those in hydrological models. We propose a new method using misfit surface information of the underlying theoretical equation for hydraulic conductivity (Mualem's Equation) to obtain an appropriate diagonal matrix, and exploit the codes in [6] to solve for the weight on the parameter misfit.

TABLE OF CONTENTS

LIST OF TABLES

LIST OF FIGURES

Chapter 1

HYDROLOGY

1.1 Soil and Water

Leading environmental scientist Daniel Hillel states, "Water is, literally, the essence of life." Its dynamic relationship with the soil forms the basis upon which all living organisms depend. Without the soil, water would be useless to plants who would have neither a means of attaching to the earth, nor a reservoir of water to draw from. There would be simply stone and sea [3].

The porous nature of soil allows plants to permeate its cavities while remaining firmly grounded, and stores water for plants to draw from. Imagine a dry pool filled with bowling balls, golf balls, shot-puts, and steelies. Then imagine the path water would take as the pool was filled from the top by a fire hose. Scale down the model and that is roughly the soil. Add to it the damming effect of clay and bedrock, the capillary action innate to water in small passages, the downward force of gravity, the ability of a soil to conduct water (hydraulic conductivity) and it becomes readily apparent how intricate a model would have to be to simulate water flow in soils.

In the last few decades our understanding of this soil–water relationship has ex-

panded dramatically, but remains vastly inadequate so far as modeling is concerned. "In many cases...the theories and equations employed in soil physics describe not the soil itself, but some ideal and well-defined model that we conjure up to simulate some aspect of the soil's behavior [3]."

One aspect of soil behavior which is especially difficult to model, and which is of great interest to scientists, is the flow of water in unsaturated soils. The unsaturated zone, or *vadose zone*, is the area between the ground surface and the water table. Here, water flow takes on several forms as it either evaporates to the air, is absorbed through plant roots, is held in place by the soil, or is transported down to the water table [3].

Knowledge of the soil-water interaction in the vadose zone allows for accurate predictions of ground water recharge rates and stream flow, among other things. These are of particular concern to hydrologists at Boise State University who conduct studies in the Dry Creek Experimental Watershed (DCEW) in an effort to improve water resource management. Located in the semi-arid southwestern region of Idaho, USA, approximately 16km northeast of the city of Boise, the DCEW is typical of the surrounding foothills of the Idaho batholith. The headwaters of the 28km^2 region begin at an elevation of 2,100m while the drainage occurs at 1,000m above sea level. Two main catchments, Dry Creek and Shingle Creek, contribute to the drainage, and are the only two perennial creeks in the DCEW, [10].

Figure 1.1 provides a graphic of the DCEW, demonstrating terrain attributes and

location of the two main catchments, Dry Creek and Shingle Creek. Data is collected at a variety of locations throughout the watershed monitoring such things as ground-water recharge, infiltration, basin precipitation, soil water distribution, stream-flow generation, and runoff over multiple scales. For the purposes of this work, infiltration and soil water distribution data will be of particular importance as they are used in predicting the unsaturated flow of water.

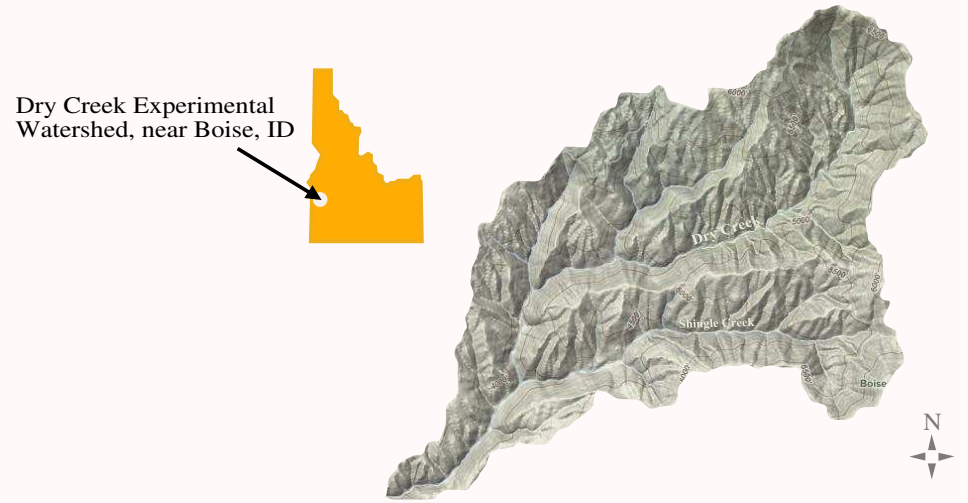

Figure 1.1.: The Dry Creek Experimental Watershed near Boise, Idaho, consists of two main drainage systems, Dry Creek and Shingle Creek. It is studied extensively by hydrologists to estimate such things as ground water recharge and stream flow. These estimates are then used to better manage water resources in the Idaho batholith.

1.2 Unsaturated Flow

According to Hillel, "Most of the processes involving soil-water interactions in the field occur while the soil is in an unsaturated condition." Unsaturated flow occurs over widely varying conditions, dependent on the timing and amounts of precipitation

as well as the type of soil. Several parameters characterize this flow. These include suction, soil wetness, and conductivity [3].

Pressure head, or *suction* in unsaturated soils, consists of the quotient of water pressure, P, and the weight density of water, γ_w, which have units $[FL^{-2}]$ and $[FL^{-3}]$, respectively. Defined by

$$\psi = \frac{P}{\gamma_w},$$

pressure head reduces to units of length, $[L]$, often denoted as *cm*. Negative during infiltration, ψ becomes zero at complete saturation of the soil, which is typically the surface of the water table. Inversely, large magnitudes of suction (very negative values of ψ) correspond to very dry soils [3]. For the non-hydrologist, pressure head may be thought of heuristically as the measure of the potential a soil has to soak up water. When it is dry it has a very large (negative) potential. When it is saturated it has no potential, or zero potential.

Volumetric water content is a ratio of the volume of water per volume of soil denoted by

$$\theta = V_w/V_s.$$

This provides a measure of the wetness of a soil. The conventional notations θ_r and θ_s stand for the minimal, or *residual water content* (dry soil), and maximal, or *saturated water content* (wet soil), respectively. As soils never become fully dry in the field, θ_r is difficult to measure, and usually must be extrapolated from available data. A distinct

relationship between the volumetric water content and pressure head exists, but there is currently no theory by which this relationship may be classified exactly [3].

A widely accepted empirical equation describing the $\theta - \psi$ relationship which is continuous for all ψ was proposed by van Genuchten (1980) [11]. Termed as the *soil-water retention curve*, it is defined by

$$\theta(\psi) = \theta_r + (\theta_s - \theta_r)[1 + (\alpha|\psi|)^n]^{1/n-1}, \tag{1.1}$$

where θ_r and θ_s denote the residual and saturated water content of the soil, respectively, and α and n are empirically fitted parameters with the specifications that $\alpha > 0$ and $n > 1$. It is used in conjunction with corresponding data of θ and ψ, where an inverse method is implemented to obtain α and n.

The soil moisture curve of best fit for a typical data set of corresponding values of θ and ψ from the DCEW is plotted in Figure 1.2. As the pressure head, ψ, tends towards zero the water content reaches the limiting value of θ_s corresponding to the maximal water content of the soil. Similarly, as the pressure head becomes large in absolute value the water content approaches the minimal limiting value of θ_r, the residual water content. Though θ is usually considered a function of ψ, the standard graphical depiction of the soil-moisture retention curve is plotted inversely as shown. Note that the data in the residual zone levels off while the fitted curve rises asymptotically. This difference between the data and fitted curve is due to the difficulties in measuring large magnitudes of ψ. Because of this, the fitted curve is

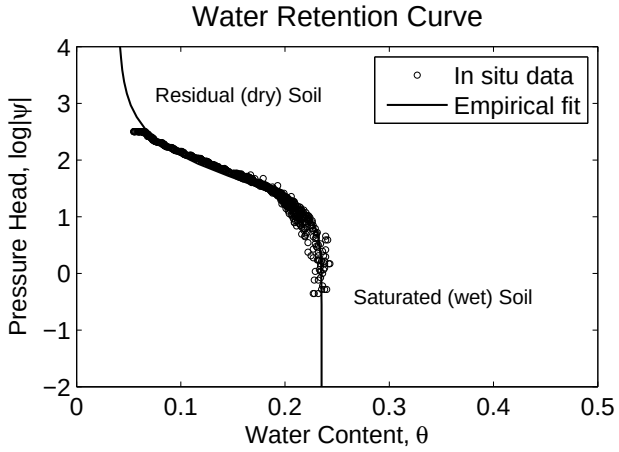

Figure 1.2.: Corresponding data of θ and ψ are fitted to obtain the curve of best fit when the soil-water retention curve is taken to be (1.1).

most often used to extrapolate information about θ_r.

Hydraulic conductivity, $K(\psi)$, is a measure of a soil's ability to conduct water. Maximal at saturation, and nearly zero at residual water contents, it depends on both the type of soil and the wetness of the soil. It is the ratio of the flux $[LT^{-1}]$ to the potential gradient (dimensionless), and thus has units of $[LT^{-1}]$, [3]. In this work it is always stated as centimeters per day $[cm/day]$.

As soil type greatly impacts conductivity properties, hydrologists generally classify soils into four main categories: clay, silt, sand, and gravel. Soils consisting mainly of sand or gravel experience very large magnitudes of conductivity near saturation. In contrast, silt and clay soil structures have relatively low values. As the soil drys this relationship is reversed. Sand and gravel shed the water rapidly, reaching residual content much more quickly than do clay or silt. Thus, for very negative values of the

pressure head, silt and clay will have relatively larger values of conductivity than sand and gravel, though these values are globally small in magnitude. Figure 1.3 taken from [3], demonstrates this relationship. The plot on the right shows two hypothetical conductivity curves, one for sand and one for clay, while the plot on the left shows their corresponding (hypothetical) soil-water retention curves. For the sandy soil the descent from maximal conductivity at saturation (K_{S1}) to minimal conductivity occurs rapidly as ψ moves away from the origin. This descent is more gradual for the clayey soil. In part, this difference is due to the texture of the soil. The clay is finer than the sand allowing water to wick through even for low water contents. The sand has large gaps, or *pore sizes* between particles allowing large amounts of water

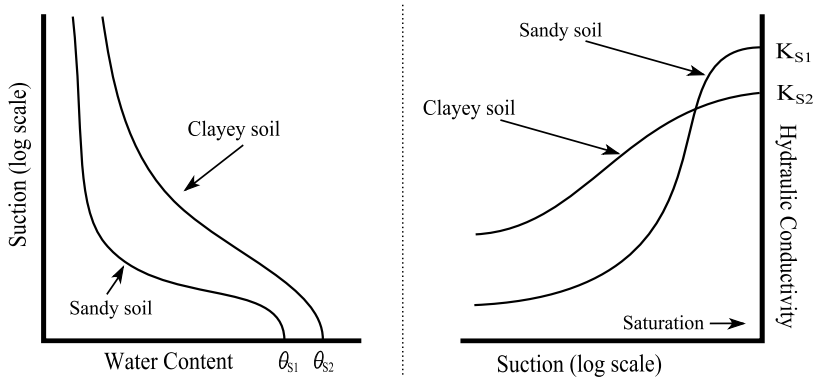

Figure 1.3.: Hypothetical curves demonstrating conductivity (right) and corresponding soil-moisture retention (left) for sand and clay soil structures.

through when the soil is nearly saturated, but traps the water because of surface tension forces as the soil drys. In the left plot, θ_{S1} and θ_{S2} denote the saturated water content for sand and clay, respectively. In both plots ψ ranges from zero at the

origin to large (negative) values at the extremity. While a clayey soil has a greater capacity to store water than a sandy soil, it takes far longer both to wet or dry.

1.3 Modeling Unsaturated Flow

A popular model used today in modeling the infiltration of water into unsaturated soils is the Richards equation (1.2). Considered "...the basic theoretical equation for infiltration into a homogeneous porous medium," [1], the usual form is

$$\partial\theta/\partial t = -\nabla \cdot [K(\psi)\nabla\psi] + \partial K/\partial z, \tag{1.2}$$

where θ is the volumetric water content, ψ is the pressure head, K is the hydraulic conductivity, z is the vertical direction, and t is the time. It is a measure of the rate of change of the volumetric water content per unit time, and is a function of space and time. Though conductivity, K, is a constant for saturated soils (denoted K_s) it is strongly dependent on ψ during unsaturated conditions [3], [1].

The Richards equation (1.2) is based on Darcy's Law and a derivation and further explanation may be found in both [3],[1]. This work focuses mainly on hydraulic conductivity, K, which is the critical element of the Richards equation. To effectively compute solutions for (1.2) reliable data or estimates of the hydraulic conductivity, K, must be obtained. Hydrologists at Boise State University are optimistic that reliable (and feasible) methods for directly measuring hydraulic conductivity in the field are

forthcoming. Currently, however, as states van Genuchten, "Reliable estimates of the unsaturated hydraulic conductivity are especially difficult to obtain, partly because of its extensive variability in the field, and partly because measuring this parameter is time-consuming and expensive" [11]. Fortunately, empirical approximations can successfully be achieved. A popular method for these approximations was proposed by van Genuchten and Y. Mualem using knowledge of the "...more easily measured soil-water retention curve" [11].

1.4 Predicting Hydraulic Conductivity

In 1976, Y. Mualem derived an equation [7] for predicting the relative hydraulic conductivity (K_r) from the soil-water retention curve (1.1). Mualem's model provides closed-form analytical expressions for hydraulic conductivity as a function of pressure head if specific hydraulic properties of the soil are known. However, suitable expressions for these hydraulic properties were not available until the later work [11] of van Genuchten (1980). His continuous form of the water retention curve (1.1) combined with the Mualem's hydraulic conductivity model [7] gave (1.3), often referred to simply as *Mualem's equation*.

Considering hydraulic conductivity K in this work instead of K_r we give Mualem's equation as

$$K(\psi; n, \alpha, K_s) = K_s \frac{\{1 - (\alpha|\psi|)^{(n-1)}(1 + (\alpha|\psi|)^n)^{1/n-1}\}^2}{(1 + (\alpha|\psi|)^n)^{(1-1/n)/2}}, \quad \psi < 0 \qquad (1.3)$$

where K_s is the measured value of saturated conductivity. The parameters n and α are obtained from the water retention curve (1.1) by fitting soil moisture and pressure head measurements. If available, n and α can also be found by fitting hydraulic conductivity data. We have introduced the notation $K(\psi; n, \alpha, K_s)$ in place of the original notation $K(\psi)$ to emphasize that K may be viewed as a function of ψ as well as a function of its parameters. We also make use of the shortened notation $K(\psi; p)$, where $p = (n, \alpha, K_s)^T$, whenever convenient.

Material	K_s $[cm/day]$
Clay	10^{-4}-10^{-2}
Silt	10^{-2}-1
Sand	10-10^3
Gravel	10^4-10^5

TABLE 1.1 Typical magnitude ranges of K_s for several soils [3].

Despite the closed-form expression for hydraulic conductivity (1.3), K is still difficult to predict. This is in part due to the large range of values the parameters obtain. The saturated hydraulic conductivity, K_s, is known to range over several orders of magnitude for homogenous soils, and the range is even greater in aggregate soils. Table 1.1 lists typical ranges of K_s for differing soil types as recorded by Hillel, [3].

The parameter α is known to range in magnitude from 10^{-2} to 10^{-3}, and the parameter n is known to range from $1 - 10$ [3],[11]. These ranges vary according to the specific soil sampled. Thus, it is critical for modeling purposes to have good *a priori* parameter knowledge about the specific soil being modeled. Table 1.2 lists

measured ranges of n, α, and K_s for the DCEW. Predicted values are taken to be the mean of the predicted values from each sample. Minimum and maximum values are taken to be the absolute min and max across all samples, respectively. These values will be used exclusively in this work.

Parameter	**Predicted**	**Minimum**	**Maximum**
n	3.3749	2.0207	4.9774
α	0.0362	0.0232	0.0692
K_s	871.4	139.7	2714.6

TABLE 1.2 Known parameter ranges and predicted values of soils in the DCEW.

Not only do the parameters vary over widely ranging magnitudes, but even relatively small perturbations in either n or α results in pronounced differences in the

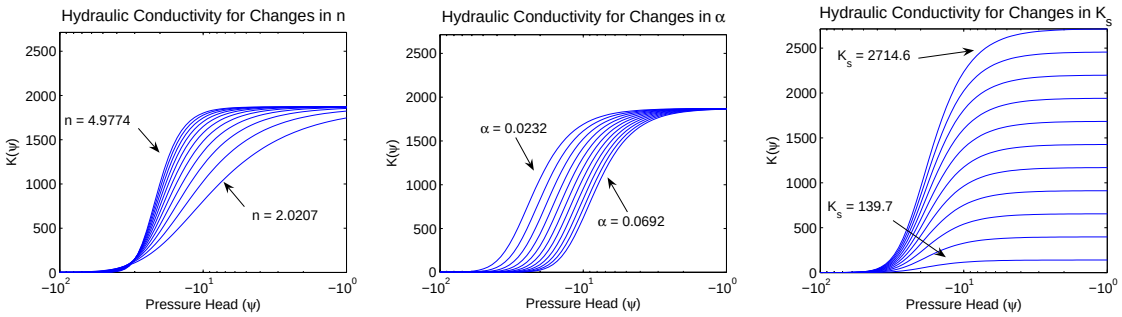

Figure 1.4.: Variations in $K(\psi; p)$ curve given movement in the parameters n, α, and K_s respectively. Labeled values denote the maximum and minimum for each parameter as recorded in Table 1.2.

prediction of K. Figure 1.4 demonstrates the effect each of the parameters n, α, and K_s has on the conductivity model (1.3). The parameter n controls the slope of the curve in the rise from residual water content conditions to saturation conditions.

The parameter α is a horizontal stretch or shrink of the position of this rise, and K_s controls the limiting value of the curve as $\psi \to 0$, which corresponds with saturation conditions. Thus the hydraulic conductivity is largest at saturation and is nearly zero for residual water contents. Explicitly, $\lim_{\psi \to 0} K(\psi; p) = K_s,$ and $\lim_{\psi \to -\infty} K(\psi; p) = 0.$

Chapter 2

LEAST SQUARES

Mualem's equation (1.3) may be used to predict hydraulic conductivity provided the parameters n, α, and K_s are specified. While K_s is obtained from laboratory experiments on representative soil samples, n and α are typically obtained by fitting measured data of θ and ψ. The RETCML method (RETention Curve – Maximum Likelihood) developed by van Genuchten et al. [4] is one of the most popular choices for this. It minimizes the following weighted least squares objective function over the parameter space of p:

$$SSQ(p) = \sum_{i=1}^{M} \left[\frac{1}{\sigma_{y_i}} (y_{i,meas}(x_i) - y_{i,model}(x_i; p)) \right]^2 . \tag{2.1}$$

Weights are chosen to be the squared inverses of the standard deviations of the error in the measurements, σ_{y_i}, which are assumed to be normally distributed.

The parameter estimates resulting from minimizing (2.1) are first tested for adequacy using a chi-square probability test where the degrees of freedom are the number of data minus the number of model parameters. Then, if sufficiently adequate, confidence regions for the parameter estimates are obtained as a function of measurement

error in the data. Thus, this method is dependent on the correct evaluation of the uncertainties in measurement error. If these uncertainties are reported to be smaller than in actuality, then the test for adequacy will be biased and the conclusion will be to reject the model. If they are larger than in actuality, then an unrealistic probability of adequacy (≈ 1) is reported [4]. The model provides the practitioner with a weighted least squares fit of the data, and corresponding confidence regions on the fit, but uses only information from data of θ and ψ and measurements of K_s. Note that if the parametric model is linear, then (2.1) may be written as

$$SSQ(p) = (d - Lp)^T C_d^{-1} (d - Lp) \tag{2.2}$$

where d is $M \times 1$, Lp is $M \times 1$, and C_p is $M \times M$ with $d_i = y_{i,meas}(x_i)$ and $(Lp)_i = y_{i,model}(x_i, p)$, and $C_{d_{ii}} = \sigma_{y_i}^2$, for $i = 1, \ldots, M$.

Recently, (2007), Mead presented a more inclusive objective function (2.3) and method of parameter estimation given both data misfit information (which RETCML uses exclusively) and parameter misfit information [5]. This method involves finding the parameter estimate $\hat{p}$ which minimizes

$$J(p) = (d - Lp)^T C_d^{-1} (d - Lp) + (p - p_o)^T C_p^{-1} (p - p_o), \tag{2.3}$$

where C_d is the covariance matrix of the measurement errors for d, C_p is the error covariance matrix for p_0, and L is a linear mapping such that Lp_0 is the mean of the

data d. The method finds the most likely C_p such that $J(\hat{p}) = M$, where M is the number of data. While the method assumes the data and parameters are independent and identically distributed, normality is not required. The basis of the theory lies in Mead's Theorem [5] which states that as M gets large, the limiting distribution of (2.3) is a χ^2 distribution with M degrees of freedom. Thus, computing C_p in this manner results in the statistically most likely C_p given the data d, data covariance C_d, and *a priori* estimate p_0.

We anticipate that estimates of hydraulic conductivity will become more abundant from laboratory testing and *in situ* data. Mead's algorithm may then be used advantageously over the RETCML method to incorporate available prior knowledge into the prediction of hydraulic conductivity, and assure a unique minimizing vector $\hat{p}$. However, a linear form of Mualem's equation is necessary.

2.1 Linear Model

In this section we linearize Mualem's equation (1.3) with respect to its parameters $p = (n, \alpha, K_s)$. We also demonstrate the sensitivity of the linear model as the point of approximation, $\tilde{p}$, is perturbed.

For a multi-variable function $f(x_1, \ldots, x_k) \to \mathbb{R}$ the linear approximation to f about the point $\tilde{x} = (\tilde{x}_1, \ldots, \tilde{x}_k)$ is given by

$$L(x_1, \ldots, x_k) = f(\tilde{x}) + \frac{\partial f}{\partial x_1}(\tilde{x})(x_1 - \tilde{x}_1) + \ldots + \frac{\partial f}{\partial x_k}(\tilde{x})(x_k - \tilde{x}_k).$$

It follows that the linear approximation, $L(\psi;p)$, to (1.3) about the parameter set $\tilde{p} = (\tilde{n}, \tilde{\alpha}, \tilde{K_s})^T$ is of the form

$$L(\psi;p) = K(\psi;\tilde{p}) + \frac{\partial K}{\partial n}(\psi;\tilde{p})(n-\tilde{n}) + \frac{\partial K}{\partial \alpha}(\psi;\tilde{p})(\alpha-\tilde{\alpha}) + \frac{\partial K}{\partial K_s}(\psi;\tilde{p})(K_s-\tilde{K_s}). \quad (2.4)$$

The computations of the partial derivatives of K in (2.4) are involved and are included in Appendix A. In order to simplify notation and write (2.4) in a form more amenable to inversion, we define the following.

$$T(\psi) = \left(\frac{\partial K}{\partial n}(\psi;\tilde{p}), \frac{\partial K}{\partial \alpha}(\psi;\tilde{p}), \frac{\partial K}{\partial K_s}(\psi;\tilde{p})\right) \quad (2.5)$$

$$S(\psi) = -\frac{\partial K}{\partial n}(\psi;\tilde{p})\tilde{n} - \frac{\partial K}{\partial \alpha}(\psi;\tilde{p})\tilde{\alpha} \quad (2.6)$$

Substitution of $T(\psi)$ and $S(\psi)$ into (2.4) gives

$$L(\psi;p) = T(\psi)p + S(\psi). \quad (2.7)$$

When the pressure head, ψ is given at M discrete points, ψ_i, $i = 1, \ldots, M$, then T and S are of dimension $M \times 3$ and $M \times 1$, respectively.

It follows that the linear model given by (2.7) gives a good approximation to the non-linear model (1.3) when $||p - \tilde{p}|| \approx 0$. We investigate the sensitivity of the linear model (2.7) as $\tilde{p}$ departs from p for the range of parameter values in Table 1.2. To demonstrate, we chose the true parameter set to be $p = (3.3749, 0.0362, 871.4)^T$,

the predicted value for each parameter, and then ranged $\tilde{p}$ over the given values in Table 1.2.

Figure 2.1 shows the resulting linear approximations when values of $\tilde{p}$ are taken at six evenly spaced points with step-size $h = (0.56, 0.0092, 514.98)^T$. Dramatic variations from the reference curve occur for large values of $||p - \tilde{p}||$ and even the

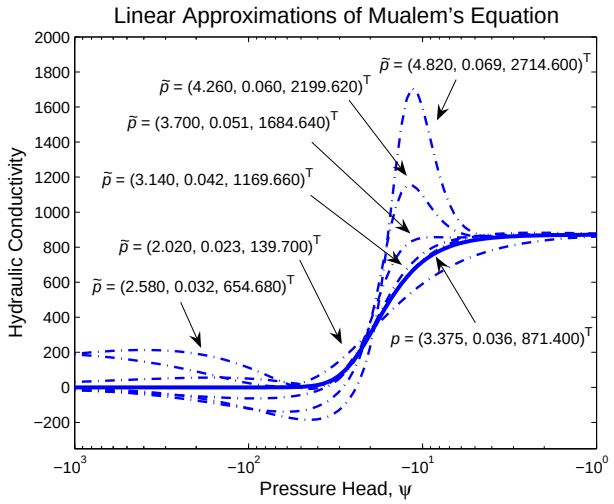

Figure 2.1.: As $\tilde{p}$ is distanced from p the linear approximation deteriorates rapidly. Only for $||p - \tilde{p}|| \approx 0$ is the approximation physically meaningful.

proper form of the hydraulic conductivity model is lost. Further, the negative values of hydraulic conductivity present in several of the linear approximations would imply that the soil actually repels water. If it rained on such a soil, the rain would hover above the surface of the soil like opposing magnets. This simply does not occur in nature. The linear model only provides a physically meaningful approximation of hydraulic conductivity when $||p - \tilde{p}|| \approx 0$.

2.2 Iterative Least Squares

As we wish to use the linear model (2.7) in the computation of (2.3) it must be that $L(\psi;\tilde{p})$ is the mean of the data d. By current assumption in hydrology, Mualem's equation (1.3) is taken as the mean of the data. Thus the linear model (2.7) may only be considered the mean of the data for a sufficiently good approximation to Mualem's equation. This only occurs if the point of approximation $\tilde{p}$ of the linear model is nearly identical to p. We show that iterated least squares used with (2.7) and good data provides a sufficient approximation when the initial estimate of $\tilde{p}$ is taken to be the maximal parameter values from Table 1.2.

Let data be given by $d = (d_1, \ldots, d_M)^T$, where $d_i = K(\psi_i; p)$ for ψ_i log-evenly spaced from -10^3 to -1 (the effective range of ψ in the field). Choosing an arbitrary $\tilde{p}$ and the same M values of ψ_i used to compute d, we construct the linear model (2.7) about the point $\tilde{p}$ and write in vector form as

$$d = Tp + S, \tag{2.8}$$

where d and S are $M \times 1$, T is $M \times 3$ and p is 3×1. Working under the assumption that $(T^T T)^{-1}$ exists, we solve (2.8) for p to obtain

$$p_{ls} = (T^T T)^{-1} T^T (d - S). \tag{2.9}$$

The parameter set p_{ls} is the least squares parameter set of best fit given the linear

model and data.

Consider the case when the synthetic data is given by the parameter set $p = (3.3749, 0.0362, 871.4)^T$, and the linear model is constructed about the point $\tilde{p} = (4.9774, 0.0692, 2714.6)^T$. Note that $\tilde{p}$ contains the maximal values from Table 1.2 for each parameter. Testing revealed that this value of $\tilde{p}$ provides the most well-conditioned version of $T^T T$. The parameter set of best fit for the chosen value of p and $\tilde{p}$ is given by $p_{ls} = (4.263, 0.05943, 868.2)^T$. We can use this least squares

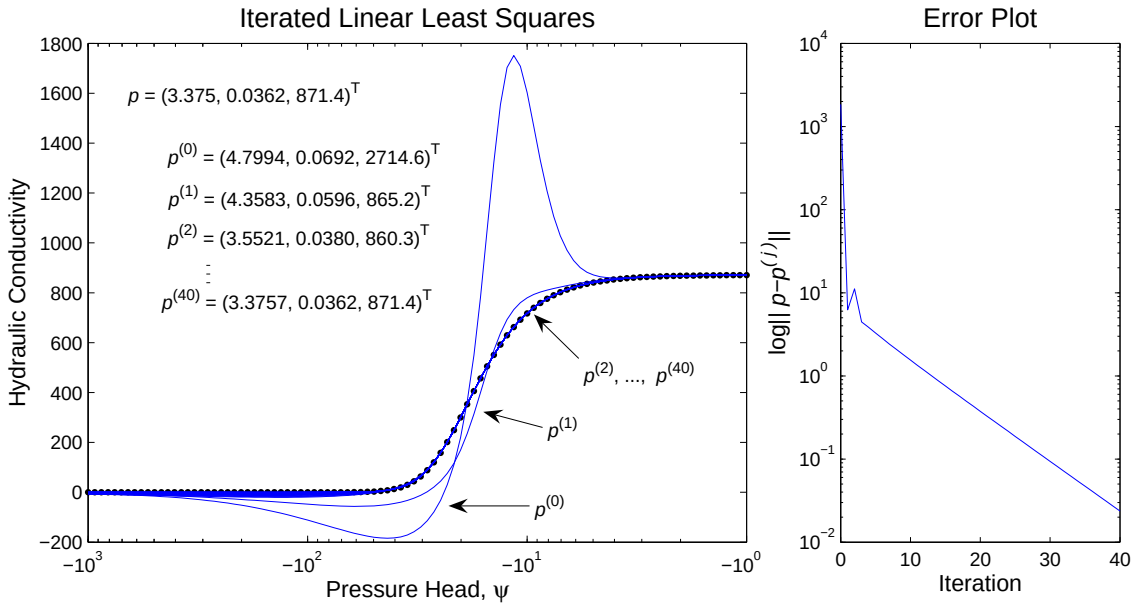

Figure 2.2.: As the linear least squares solution is iterated, the linear approximation (lines) simulates the non-linear form of the data (dots).

estimate p_{ls} to update the linear model by letting $\tilde{p} = p_{ls}$ and solving (2.9) again for p_{ls}. Iterating this process allows the data to pull the initial parameter estimate $\tilde{p}$ as close as desired to the true solution p. Thus, iterating simulates the non-linear

behavior of Mualem's equation, and provides a sufficient approximation such that the linear model may be considered as the mean of the data. Results for this case are depicted in Figure (2.2) where the iterates $p^{(0)}, p^{(1)}, \ldots, p^{(40)}$ denote the curve given by the linear model $L(\psi; p)$, i.e. equation (2.7), approximated about the iterate $p^{(j)}$.

Similar results were obtained for values of p throughout the domain of measured values given by Table 1.2. So long as $\tilde{p}$ was initially chosen to be the maximal parameter values the iterations eventually converged to the true solution. Convergence was slowest for p with near minimal values of n due to poor conditioning of $T^T T$. This suggests the need for some sort of regularization of $T^T T$ to ensure convergence for all choices of p.

2.3 Objective Function

To incorporate all prior knowledge about the parameters and ensure the minimization problem is well posed we propose Mead's model (2.3) where the mapping L is given by the linear model (2.7), i.e.

$$J(p) = (d - (Tp + S))^T C_d^{-1} (d - (Tp + S)) + (p - p_0)^T C_p^{-1} (p - p_0). \tag{2.10}$$

The prior information p_0 can be found from laboratory experiments while the data d comes from conductivity measurements in the field with corresponding error covariance C_d. Due to the quadratic nature of (2.10), the unique minimizing parameter set

$\hat{p}$ may be found by solving

$$J'(p) = -2T^T C_d^{-1} + 2T^T C_d^{-1} Tp + 2T^T C_d^{-1} S + 2C_p^{-1} p - 2C_p^{-1} p_0 = 0. \tag{2.11}$$

This provides the solution

$$\hat{p} = p_0 + (T^T C_d^{-1} T + C_p)^{-1} T^T C_d^{-1} (d - (Tp + S)). \tag{2.12}$$

Both C_d and C_p are covariance matrices, and hence are symmetric positive definite [5]. Thus, the difficulty with the simple least squares solution (2.9) caused by inverting the sometimes ill-conditioned $(T^T T)$ is overcome by inverting $(T^T C_d^{-1} T + C_p)$ instead. The effect of the magnitudes of both $||C_d||$ and $||C_p||$ can be seen in (2.10) where it is evident that $||C_p||$ or $||C_d||$ being large in magnitude implies very little confidence in the parameters or data, respectively. Similarly, $||C_p||$ or $||C_d||$ being small in magnitude implies great confidence. The covariance matrix C_d will be available from corresponding field measurements. Computing C_p, the covariance of the *a priori* initial parameter estimate p_0, is more difficult as it depends on how close p_0 is to the unknown mean solution of the parameters, assuming the parameters to be stochastic.

Mead's method is a deterministic approach which solves for the matrix C_p such that $J(\hat{p}) = M$, where M is the number of data and $\hat{p}$ is the minimizing parameter set for (2.10). This method was used to solve several benchmark problems more efficiently than either of the well known L-curve, or general cross-validation methods [5]. It has

also been successfully used to fit data for the soil-water retention curve [9]. Despite the success, robust codes for the algorithm, which requires solving for $M \times M$ unknowns with only M equations, are still being actively researched.

Currently, robust algorithms have been established for C_p restricted to a diagonal matrix D [6]. In these methods a Newton root finding technique is used to solve for a scalar λ such that $J(\hat{p}) = M$ when $C_p = \lambda D$. Typically, the operator D is taken to be an approximation to the l^{th} order derivative, $l = 0, 1, 2$, and equally weights each parameter. As the hydrologic parameters n, α and K_s each differ by an order of magnitude (Table 1.2) it is necessary that D is adjusted to properly reflect the magnitude of each parameter. In the following chapter we propose using a new method involving misfit surface information for finding a diagonal matrix D which is appropriately scaled in each coordinate.

Chapter 3

WEIGHT SELECTION

In Chapter 2 we introduced the objective function (2.10) which provides the optimal fit of *in situ* data and corresponding laboratory results if C_d and C_p are specified correctly. Though C_d may be obtained from repeated measurements of the data, computing the covariance of the parameters is more difficult as the underlying *a priori* distribution is unknown and not directly measurable [5]. Though Mead's Algorithm [5] computes C_p so that it satisfies distribution expectations on the cost function (2.10), robust numerical codes are currently only available for the restricted case of $C_p = \lambda D$, where D is given, and λ (scalar) is obtained by the Newton method of Mead and Renaut [6]. This restricted case only allows for a constant weighting on the parameter misfit and is insufficient for parameters such as n, α, and K_s which differ by several orders of magnitude. We propose here that a diagonal matrix which appropriately scales each parameter may be obtained from misfit surface information of Mualem's equation (1.3). This scaling depends on a single parameter c which may be found using existing codes in [6].

3.1 Misfit Surface

The misfit surface provides a measure of the error δK which is incurred in hydraulic conductivity K when an initial parameter p_0 is perturbed by $\delta p = p - p_0$. Thus, for a given tolerance of δK the misfit surface may be used to determine the corresponding δp. This δp is the standard deviation for p_0 that we use to decide the appropriate diagonal scaling matrix, i.e. $D = diag(\delta n, \delta\alpha, \delta K_s)$, from which we form C_p. Though this C_p does not tell us the error in the initial parameter estimate it does scale the error in the parameters appropriately.

We calculate the misfit surface by computing the hydraulic conductivity, $K(\psi_i; p)$, at M distinct values of ψ_i, $i = 1, \ldots, M$. Another parameter set, $p + \delta p$, is chosen and $K(\psi_i; p + \delta p)$ is computed for the same M values of ψ_i. The error between the two curves is measured by taking the log of their two norm misfit, i.e.

$$c(\delta p) = \log ||K(\psi_1, \ldots, \psi_M; p) - K(\psi_1, \ldots, \psi_M; p + \delta p)||_2, \quad \delta p \neq \vec{0}. \tag{3.1}$$

This produces a single real number c representing the log of the error in hydraulic conductivity K generated by the perturbation of δp from p. We plot the error, or misfit surface, for evenly spaced δp throughout the domain of the parameters as listed in Table 1.2.

For visualization purposes, Figure 3.1 considers only variations in α and n, while holding K_s constant. Error levels corresponding to $c = 1, 2, 2.5, 3, 3.5$ are plotted as

well as the corresponding level curves. It is readily seen that even small movements away from α and n result in large amounts of error. However, this is without

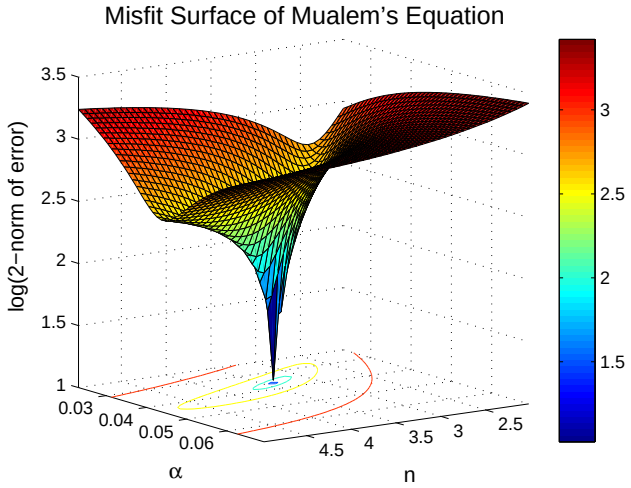

Figure 3.1.: Misfit surface of Mualem's equation when K_s is held constant and $p = (3.3749, 0.0362, 871.4)^T$.

reference to the original situation. To give a better feel of the meaning of the error values depicted, consider Figure 3.2 where the corresponding conductivity curves (or families of curves) are plotted. The curve designated by $K(\psi; p)$ lies directly on the curve corresponding to an error level of $c = 1$. The different error regions surrounding this true curve represent the resulting family of conductivity curves given by $K(\psi; p + \delta p)$ satisfying the given error levels depicted in Figure 3.1. An error level of $c = 2$ represents relative accuracy, while an error level greater than $c = 3$ is likely not very informative. It should be noted that viewing the error regions in the conductivity plot allows for all three parameters to be varied simultaneously. Thus more information is presented in Figure 3.2 than in Figure 3.1.

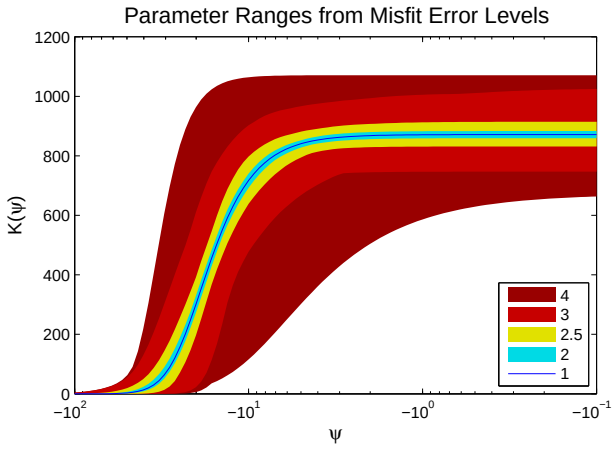

Figure 3.2.: Error regions corresponding to $c = 1, 2, 2.5, 3, 4$ on the Misfit Surface plot (Figure 3.1) are given here as conductivity curves. Note that K_s is also varied.

The level curves in Figure 3.1 are oddly shaped and difficult to define. This creates difficulties in retrieving information about the amount of error the parameters may obtain while (3.1) remains within a specified tolerance. If the misfit surface is to be used to obtain standard deviations for the parameters, then some smoothing of the level curves must be achieved. We accomplish this in the following section by using the first order approximation to the misfit surface.

3.2 First Order Approximation of Misfit Surface

We demonstrate that a first order approximation to the misfit surface may be used to advantageously reshape the level curves defined by (3.1). These simplified curves both adequately approximate the true level curves and provide useful parameter bounds for a given tolerance of the misfit. This information may then successfully be used to

compute the appropriate diagonal values of D.

Consider a function $f : \mathbb{R} \to \mathbb{R}$. The first order approximation to f about some point $\tilde{x}$ in the domain of f is given by

$$f(x) \approx f(\tilde{x}) + f'(\tilde{x})(x - \tilde{x}).$$

Evaluating the first order approximation at $x = \tilde{x} + h$ we obtain,

$$f(\tilde{x} + h) \approx f(\tilde{x}) + h \cdot f'(\tilde{x}).$$

Thus, the misfit between $f(\tilde{x} + h)$ and $f(\tilde{x})$ can be approximated by $h \cdot f'(\tilde{x})$, i.e.

$$f(\tilde{x} + h) - f(\tilde{x}) \approx h \cdot f'(\tilde{x}).$$

For our purposes, we have that hydraulic conductivity $K(\psi; p + \delta p)$ can be approximated about the parameter set $\tilde{p} = p$ by the linear approximation to Mualem's equation (2.7) as

$$K(\psi; p + \delta p) \approx T(\psi)(p + \delta p) + S(\psi) \tag{3.2}$$

$$= T(\psi)\delta p + T(\psi)p + S(\psi). \tag{3.3}$$

Since the linear model $T(\psi)p + S(\psi)$ was approximated about the point $\tilde{p} = p$ we have that the linear approximation $L(\psi; p)$ and the non-linear Mualem's equation $K(\psi; p)$

agree, i.e. by (2.4) and (2.7) we have that

$$L(\psi; p) = K(\psi; p) = T(\psi)p + S(\psi).$$

So the misfit between $K(\psi; p+\delta p)$ and $K(\psi; p)$ may be obtained by rearranging (3.3) to obtain

$$K(\psi; p + \delta p) - K(\psi; p) \approx T(\psi)\delta p.$$

From this we may compute the misfit error across all M values of ψ as

$$c(\delta p) = \log ||T\delta p||_2, \quad \delta p \neq 0. \tag{3.4}$$

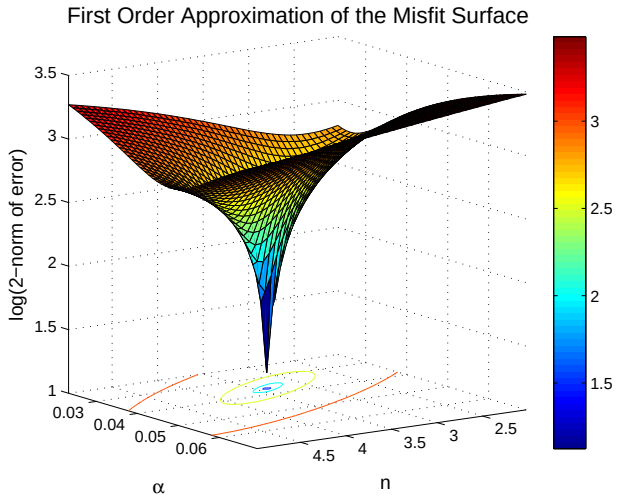

Figure 3.3.: Comparing the first order approximation to the true misfit surface (Figure 3.1) witnesses the approximation is satisfactory for $||\delta p||$ small.

For each perturbation $p + \delta p$ in the domain of the parameters we may compute

an approximation to its misfit surface using only the perturbation δp and the one time computation of T approximated about the point p. (The matrix T must be recomputed for different choices of p however.) Using this method produces the misfit surface depicted in Figure 3.3 which, though clearly a first order approximation, performs well against the true misfit for small values of $||\delta p||$.

3.3 Misfit Surface for Weight Selection in WLS

In Figure 3.4 we use a two-dimensional contour plot of the linear approximation to the misfit surface (Figure 3.3) to demonstrate how values for each coordinate of the diagonal matrix D will be obtained. We use the first order approximation advantageously over the true misfit both because of the simplified computations and

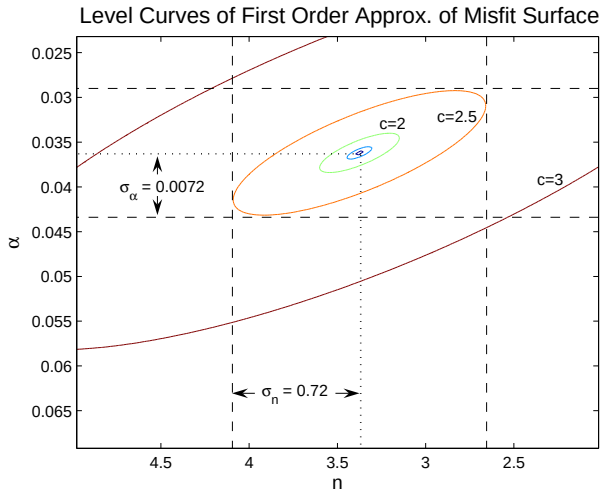

Figure 3.4.: A box is centered around the point of reference p to obtain standard deviations of the parameters n and α for the error level of 2.5 on the misfit surface. (K_s is held constant.)

the more well behaved level curves. Recall that for visualization purposes of the misfit K_s is held constant while both α and n are perturbed away from the given reference values of $n = 3.375$ and $\alpha = 0.0362$. This provides the misfit surface, whose first order approximation contours corresponding to $c = 1, 1.5, 2, 2.5, 3$ are depicted. We center a rectangle around the reference point $n = 3.375$ and $\alpha = 0.0362$ which contains the error contour of 2.5, and provides standard deviations for the parameters n and α as 0.72 and 0.0072, respectively. Thus the standard deviations corresponding to the level curve $c = 2.5$ for each parameter n, α, and K_s may be written in vector form as $\sigma_{2.5} = (0.72, 0.0072, 0)^T$, as there is no variation in K_s. We could define $C_p = diag(\sigma^2_{2.5})$. However, it is not clear that $c = 2.5$ is the correct choice for the optimal parameter estimate.

We observed a relationship between the standard deviation and the level curves that allowed retrieval of the standard deviation for a given error level without reference to the misfit surface. Since the misfit surface had been reduced to a first order approximation, the level curves became concentric ellipses. Further, the standard deviations for the level curve $c = 2$ are one third the values obtained for $c = 2.5$. Inversely, the standard deviations for the level curve $c = 3$ are three times those of $c = 2.5$. In general, standard deviations for a given level curve c may be obtained by the relation

$$\sigma_c = 3^{2(c-d)}\sigma_d,$$

where d is chosen and σ_d is known. This provides the parameter weight as $C_p =$

$\left(3^{2(c-d)}\right)^2 diag(\sigma_d^2)$, so that the only difficulty is in determining c so that $J(\hat{p}) \approx M$. These preliminary results for the two dimensional case with K_s held constant can be described in detail with Figures such as 3.4, but cannot be used in practice due to the large variation typical of K_s.

Perturbing K_s makes the level curves in Figure 3.4 shift and contract. When all three parameters, n, α, and K_s are perturbed simultaneously, the level curves are three dimensional ellipsoids. Standard deviations are obtained for all three parameters similarly to the two-dimensional case by placing a bounding box around the ellipsoid which is centered around the point of reference p. For example, the standard deviation for each parameter corresponding to the minimum error contour of $c = 1$ is given by

$$\sigma_1 = (0.0235, 0.00022, 1.4)^T. \tag{3.5}$$

Further computations witnessed that standard deviations defining a bounding box for the general contour level c may be obtained by $\sigma_c = f(c)\sigma_d$, where

$$f(c) = \left(\frac{35}{11}\right)^{2(c-d)}. \tag{3.6}$$

It follows that we may define $D = diag(\sigma_d^2)$ and solve for c such that $J(\hat{p}) \approx M$ when $C_p = f(c)^2 D$.

To minimize computations in the search for the optimizing value of c, we exploit

the following result [5]

$$J(\hat{p}) = h^T P^{-1} h, \tag{3.7}$$

where $h = d - (Tp_0 + S)$, and $P = TC_pT^T + C_d$. Note that $J(\hat{p})$ may now be computed without $\hat{p}$. This eliminates the need to solve for $\hat{p}$ at each iteration of the minimization process. Thus, the problem has been reduced to finding c such that

$$F(c) = h^T P^{-1} h - M = 0. \tag{3.8}$$

This is the root finding problem of [6] for which robust codes are already in place. It has already been shown that the Newton steps converge for the case of λD. However, future work involves showing this holds when λD is replaced with $f(c)^2 D$, where $f(c)$ is given by (3.6), and D is defined by standard deviations obtained from the misfit surface as in (3.6).

3.4 Synthetic Data and Testing

Previously, we selected the objective function of Mead (2.10) advantageously over that of RETCML (2.1) in order to incorporate available *a priori* information about p_0 into the prediction of hydraulic conductivity. This required knowledge of the prior covariance of the parameters C_p, but such knowledge is difficult to obtain from measured data. Instead, we propose using a linear approximation to the misfit surface to obtain a generalized diagonal weight $C_p = f(c)^2 diag(\sigma_d)$ with $f(c)$ defined by (3.6).

This reduced the problem from solving for an entire matrix, to solving for a single constant c using established code from [6]. We now demonstrate that approximating C_p in this manner satisfactorily blends a best fit of data and *a priori* parameter knowledge into an optimal solution $\hat{p}$ of (2.10) with corresponding confidence regions.

As the minimum value of (2.10) follows a χ^2 distribution with M degrees of freedom, we wish to select the covariance on the parameters, C_p, to be those values of the standard deviations which produce a solution $\hat{p}$ to (2.10) such that $J(\hat{p}) \approx M$. Because M is assumed to be large, it follows that the χ^2 distribution may be approximated by a normal distribution with mean M and standard deviation $\sqrt{2M}$. Thus, using the z-statistic at the 0.1 significance level, we have that so long as $J(\hat{p}) \in [M - 3.64, M + 3.64]$ the choice of C_p is statistically likely given the data, data weight, and initial parameter estimate [5].

To test our method we construct synthetic data for hydraulic conductivity, K, as follows. Let data be given by $d = (d_1, \ldots, d_M)^T$, where $d_i = K(\psi_i; p)$ for ψ_i log-evenly spaced from -10^2 to -1, and $p = (3.375, 0.0362, 871.4)^T$, the predicted values for each parameter. The perfect data is then blurred by adding normally distributed random variates according to a specified standard deviation, namely C_d. Thus, $d_i = d_i + \epsilon_i$, where ϵ_i is a normal random variate with mean zero and standard deviation given by the square root of the i^{th} diagonal element of C_d. Similarly, the initial *a priori* estimate p_0 (to be obtained through laboratory experiments) was taken to be p blurred in a similar manner as the data. We then solve for c, and hence C_p using the code of

Mead and Renaut as defined in [6]. Error bounds for $\hat{p}$ are then computed by means of [8],

$$cov(\hat{p}) = C_p - C_p T^T P^{-1} T C_p. \tag{3.9}$$

We summarize our findings with the following four descriptive cases.

Case 1. The *a priori* estimate p_0 is chosen so that a feasible solution c exists which satisfies (3.8) such that $J(\hat{p}) = M$ and the elements of C_p are of reasonable magnitudes. Hence, the results are meaningful and posterior confidence regions on $\hat{p}$ contain the true solution from which the data and initial parameter estimate were blurred. Figure 3.5 depicts such a situation.

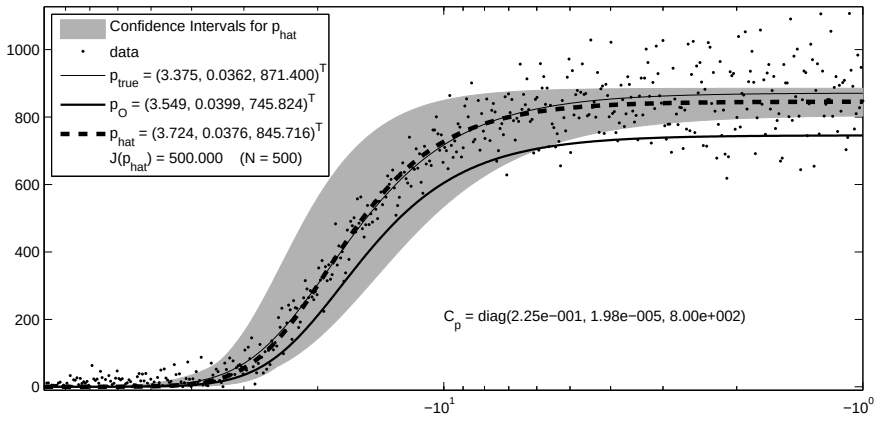

Figure 3.5.: The weighted least squares fit (dashed lines) against the corresponding data, initial parameter estimate p_0 (thick solid line), and true solution (thin solid line) from which the data were blurred.

Case 2. The initial estimate p_0 is chosen so that a feasible solution c exists which satisfies (3.8) with $J(\hat{p}) = M$, but C_p is small in magnitude. This causes the resulting confidence region to be overly optimistic and miss the true solution. Figure 3.6 shows

such a case. Such results are not unique to this method. RETCML faces similar problems when the errors in the data measurements are reported to be larger than in actuality and are discuess further in [11].

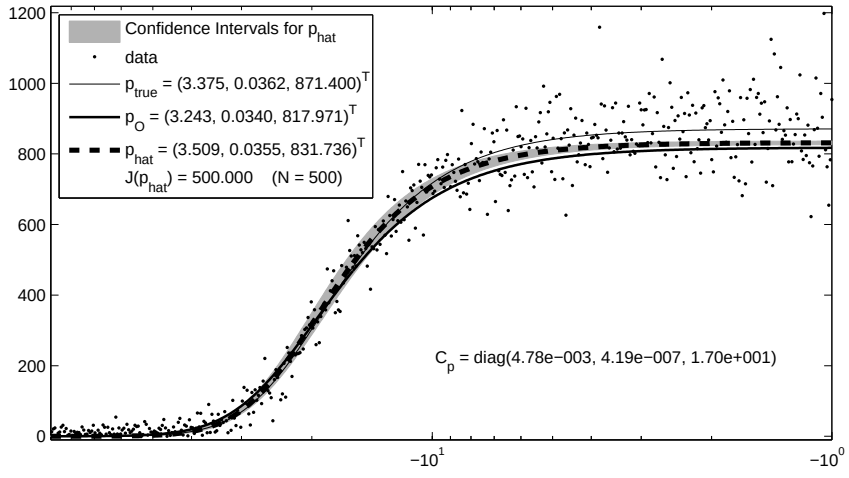

Figure 3.6.: Overly optimistic confidence regions are the result of small values of C_p, and the confidence region fails to capture the true solution.

We suggest that the practitioner use available *a priori* knowledge to try different values of p_0 and then use (3.8) with the algorithm of Mead and Renaut [6] to weight the estimate. The practitioner should use their discretion in accepting the results when the confidence regions on the solution $\hat{p}$ are small. Also, they should be aware of the following two cases where the results are inconclusive.

Case 3. The estimate p_0 is chosen so that no feasible solution c exists which satisfies (3.8). In this case C_p is extremely large and $J(\hat{p}) > M + 3.64$. Thus, we reject the results with the conclusion that the initial parameter estimate p_0, data, and data weight do not accurately reflect the same soil sample. As C_p large, the resulting

confidence region extends across the entire parameter space. See Figure 3.7.

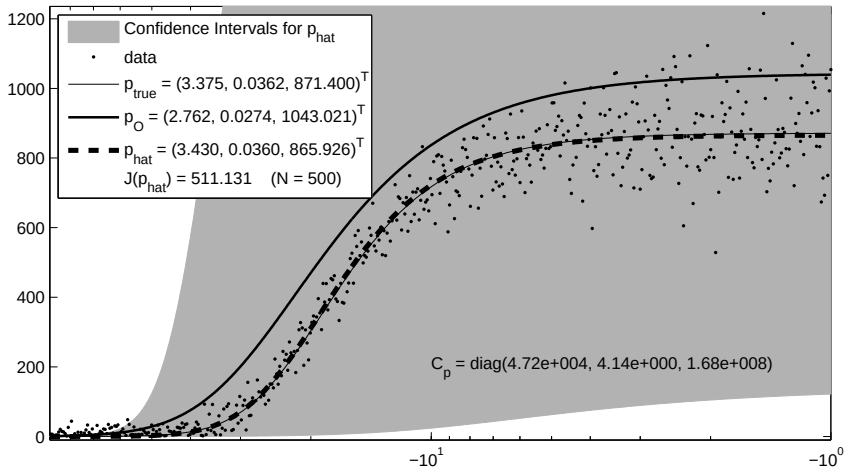

Figure 3.7.: In an effort to get $J(\hat{p}) < M + 3.64$ the algorithm had to zero out the parameter misfit term by making C_p extremely large. This results in confidence regions which cover the entire parameter space. The results are thus inconclusive.

Case 4. The estimate p_0 is chosen so that no feasible solution c exists which satisfies (3.8), but in this case C_p has elements nearly identical to zero and $J(\hat{p}) < M - 3.64$. The results are again rejected as improbable. The weight C_p^{-1} was made extraordinarily large in an attempt to achieve $J(\hat{p}) \approx M$. Thus, the optimal solution is necessarily identical to p_0 in order to minimize (2.10) by eliminating the large parameter misfit weight. As a result of the extremely small values of C_p the confidence regions on the solution $\hat{p}$ are smaller than the thickness of the line depicting the solution in Figure 3.8.

From the results of cases 3 and 4 we conclude that the use of Matlab's *fsolve*, which was used here, is not sufficiently robust and that the full algorithm of Mead and Renaut must be implemented to ensure convergence. It is worth noting however

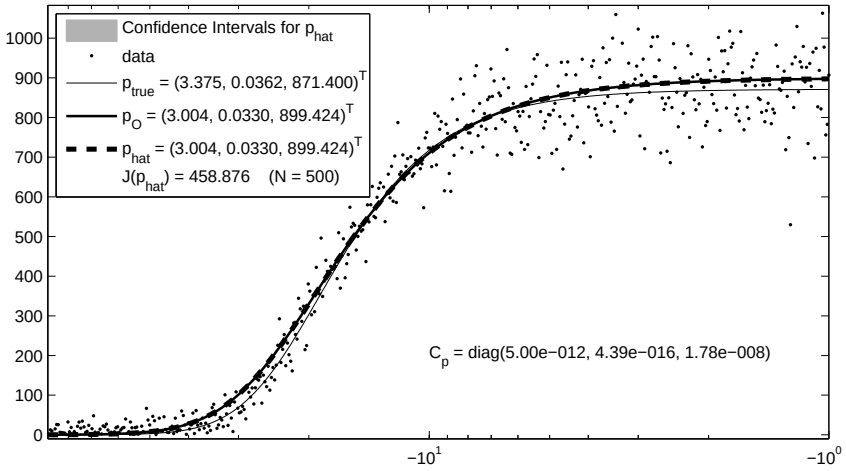

Figure 3.8.: The value of $J(\hat{p})$ is smaller than expected witnessing that the objective function (2.10) is placing too much weight on the parameter misfit, and should be rejected.

that whenever $J(\hat{p}) < M - 3.64$ it follows that C_p is nearly zero, and that C_p is extremely large whenever $J(\hat{p}) > M + 3.64$.

Chapter 4

CONCLUSIONS

To model ground water flow using the Richards equation (1.2), accurate estimates of hydraulic conductivity are necessary. Currently, RETCML is usually implemented to obtain estimates of hydraulic conductivity from information about the soil-water retention curve (1.1), and the measured value of saturated conductivity K_s. When *in situ* data for hydraulic conductivity become available, RETCML may also be used to obtain a weighted least squares fit of the data using measurement errors as weights. However, as both *in situ* data and laboratory estimates of the parameters will be available, we proposed using Mead's objective function (2.3) advantageously over RETCML in order to incorporate all knowledge available into the prediction of hydraulic conductivity.

Robust numerical codes for implementing Mead's algorithm are currently only available for a diagonal version C_p of the form λD, where D is typically an approximation to the l^{th} order derivative. Due to the differing magnitudes of each of the hydraulic parameters n, α, and K_s, it was necessary to find a diagonal matrix D which was properly scaled in each coordinate. This was done using the first order approximation to the misfit surface. Because of the nature of this misfit surface, the

standard deviations of the parameters corresponding to any given error level could be obtained from a single vector (3.5) according to the relationship in (3.6). Thus, the covariance C_p was determined to be of the form $f(c)^2 D$, where $D = diag(\sigma_d^2)$.

Evaluating the objective function (2.10) for the resulting optimal solution $\hat{p}$ serves as a statistical test for the adequacy of the solution. For the significance level of 0.1, we reject the solution whenever $J(\hat{p}) > M + 3.64$ or $J(\hat{p}) < M - 3.64$ due to its extremely low probability of occurrence. This provides a control for the practitioner to recognize when the objective function (2.10) should not be used. Whenever a probable solution is obtained, confidence regions of the optimal parameter estimate $\hat{p}$ usually correctly define the certainty of the estimate. However, at times this estimate is too optimistic and the true solution is not contained within the provided confidence regions. Thus, the practitioner should be wary when confidence regions are small. When the method is successful the results may be used to more accurately predict hydraulic conductivity, and hence solutions to the Richards equation, using both *in situ* and laboratory data until more robust codes for Mead's full algorithm are derived.

REFERENCES

[1] S. Lowrence Dingman. *Physical Hydrology.* Prentice Hall, Second edition, 2002. Academic Press, San Diego, CA, 1998.

[2] C. W. Fetter. *Applied Hydrogeology.* Prentice Hall, Fourth edition, 2001.

[3] Hillel, Daniel. *Environmental Soil Physics.*

[4] K.J. Hollenbeck, J. Simunek, M. Th. van Genuchten. RETCML: Incorporating maximum-likelihood estimation principles in the RETC soil hydraulic parameter estimation code. *Computers & Geosciences*, vol. 26, pp. 319–327, 2000.

[5] J. Mead. Parameter Estimation: A new approach to weighting a priori information. *Journal of Inverse Ill-posed Problems*, vol. 15, pp. 1-21, 2007.

[6] J. L. Mead, R. A. Renaut. A Newton root-finding algorithm for estimating the regularization parameter for solving ill-conditioned least squares problems. *Inverse Problems* p. 175-194, Vol. 16, No.2, 2008.

[7] Y. Mualem. A new model for predicting the hydraulic conductivity of unsaturated porous media. *Water Resource Research*, 12:513-522, 1976a.

[8] A. Tarantola. *Inverse Problems Theory and Methods for Model Parameter Estimation.* (SIAM) p 342, 2005.

[9] R. Treneva. Parameter Estimation in Soil Hydraulic Models. Masters Thesis, Boise State University, Boise, Idaho, USA, 2007.

[10] C. J. Williams. Characterization of the Spatial and Temporal Controls on Soil Moisture and Streamflow Generation in a Semi-Arid Headwater. Masters Thesis, Boise State University, Boise, Idaho, USA, 2005.

[11] M. Th. van Genuchten. A Closed-form Equation for Prediciting the Hydraulic Conductivity of Unsaturated Soils. *Soil Science Society of America Journal*, 44:892-898, 1980.

Appendix A

COMPUTATIONS FOR LINEARIZING MUALEM'S EQUATION

The following computations are referenced in the text just after Equation (2.4), and demonstrate the linearization of Mualem's Equation (1.3). A notation change for clarity is implemented so that $\tilde{p} = p_0$. Recall that the linear form of Mualem's Equation is given by

$$L(\psi;p) = K(\psi;p_o) + \frac{\partial K}{\partial n}(\psi;p_o)(n-n_o) + \frac{\partial K}{\partial \alpha}(\psi;p_o)(\alpha-\alpha_o) + \frac{\partial K}{\partial K_s}(\psi;p_o)(K_s - K_{s_o}). \tag{A.1}$$

The partial derivative of $K(\psi;p_o)$ with respect to n is of the form,

$$\frac{\partial K}{\partial n}(\psi;p_o) = K_{s_o}\frac{\left(D(\psi)\cdot\frac{\partial N(\psi)}{\partial n} - N(\psi)\cdot\frac{\partial D(\psi)}{\partial n}\right)}{(D(\psi))^2},$$

with the following values for $D(\psi)$ and $N(\psi)$ and their partial derivatives with respect to the parameter n.

$$\begin{aligned}
D(\psi) &= [1+(\alpha_o|\psi|)^{n_o}]^{(1-1/n_o)/2},\\
N(\psi) &= \{1-(\alpha_o|\psi|)^{n_o-1}[1+(\alpha_o|\psi|)^{n_o}]^{1/n_o-1}\}^2\\
\frac{\partial D(\psi)}{\partial n} &= n_o^{-2}/2[1+(\alpha_o|\psi|)^{n_o}]^{(1-1/n_o)/2}\cdot\log(1+(\alpha_o|\psi|)^{n_o})\cdot(\alpha_o|\psi|)^{n_o}\log(\alpha_o|\psi|)\\
\frac{\partial N(\psi)}{\partial n} &= -2\{1-(\alpha_o|\psi|)^{n_o-1}[1+(\alpha_o|\psi|)^{n_o}]^{1/n_o-1}\}\cdot(g(\psi)\frac{\partial h(\psi)}{\partial n} + \frac{\partial g(\psi)}{\partial n}h(\psi))
\end{aligned}$$

Also, we have the following values for these intermediate substitutions.

$$\begin{aligned}
g(\psi) &= (\alpha_o|\psi|)^{n_o-1}\\
h(\psi) &= [1+(\alpha_o|\psi|)^{n_o}]^{1/n_o-1}\\
\frac{\partial g(\psi)}{\partial n} &= (\alpha_o|\psi|)^{n_o-1}\log(\alpha_o|\psi|)\\
\frac{\partial h(\psi)}{\partial n} &= -n_o^{-2}[1+(\alpha_o|\psi|)^{n_o}]^{1/n_o-1}\log(1+(\alpha_o|\psi|)^{n_o})\cdot(\alpha_o|\psi|)^{n_o}\log(\alpha_o|\psi|).
\end{aligned}$$

Piecing these several substitutions back together provides $\frac{\partial K}{\partial n}(\psi;p_o)$.

Similarly, the partial derivative of $K(\psi; p_o)$ with respect to α is of the form,

$$\frac{\partial K}{\partial \alpha}(\psi; p_o) = K_{s_o} \frac{\left(D(\psi) \cdot \frac{\partial N(\psi)}{\partial \alpha} - N(\psi) \cdot \frac{\partial D(\psi)}{\partial \alpha} \right)}{(D(\psi))^2},$$

with the following values for $D(\psi)$ and $N(\psi)$ and their partial derivatives with respect to the parameter α.

$$\begin{aligned}
D(\psi) &= [1 + (\alpha_o|\psi|)^{n_o}]^{(1-1/n_o)/2}, \\
N(\psi) &= \{1 - (\alpha_o|\psi|)^{n_o-1}[1 + (\alpha_o|\psi|)^{n_o}]^{1/n_o-1}\}^2 \\
\frac{\partial D(\psi)}{\partial \alpha} &= (1 - 1/n_o)/2[1 + (\alpha_o|\psi|)^{n_o}]^{(1-1/n_o)/2-1} \cdot n_o(\alpha_o|\psi|)^{n_o-1})|\psi| \\
\frac{\partial N(\psi)}{\partial \alpha} &= -2\{1-(\alpha_o|\psi|)^{n_o-1}[1 + (\alpha_o|\psi|)^{n_o}]^{1/n_o-1}\} \cdot (g(\psi)\frac{\partial h(\psi)}{\partial \alpha} + \frac{\partial g(\psi)}{\partial \alpha}h(\psi))
\end{aligned}$$

Also, we have the following values for these intermediate substitutions.

$$\begin{aligned}
g(\psi) &= (\alpha_o|\psi|)^{n_o-1} \\
h(\psi) &= [1 + (\alpha_o|\psi|)^{n_o}]^{1/n_o-1} \\
\frac{\partial g(\psi)}{\partial \alpha} &= (n_o - 1)(\alpha_o|\psi|)^{n_o-2}|\psi| \\
\frac{\partial h(\psi)}{\partial \alpha} &= (1/n_o - 1)[1+(\alpha_o|\psi|)^{n_o}]^{1/n_o-2} \cdot n_o(\alpha_o|\psi|)^{n_o-1} \cdot |\psi|.
\end{aligned}$$

When pieced back together, these values provide $\frac{\partial K}{\partial \alpha}(\psi; p_o)$. As $K(\psi; p_o)$ is already linear with respect to K_s, we simply note that in (A.1),

$$K(\psi; p_o) \quad \text{and} \quad \frac{\partial K}{\partial K_s}(\psi; p_o)(K_s - K_{s_o})$$

reduce to $K(\psi; n_o, \alpha_o, K_s)$.